

# CFD Modeling of Airfoil of wind turbine under different effect of operating conditions

Abdalsalam Muftah

*e-mail: salamgader@su.edu.ly*

*Mechanical Engineering Department, Faculty of Engineering, Sirte University*

## Abstract

Wind energy has been attracting more and more attentions due to its clean and renewable source. The aerodynamic characteristic of wind turbine airfoil directly affects the turbine efficiency. In this paper, Computational fluid dynamics (CFD) analysis of the two-dimensional air flow over a wind turbine NACA 2414 airfoil at various angles of attack and operating Reynolds number are presented. Aerodynamics airfoil performance which were represented by Lift Coefficient (Cl), Drag Coefficient (Cd) and Lift-to-Drag ratio (Cl/Cd) are determined. The geometry of the airfoil is created using NACA parametric curves in COMSOL Multiphysics Design Modeler. CFD analysis is carried out using Comsol models at various angles of attack starting from  $-5^\circ$  to  $15^\circ$ , and at seven various operating condition of Reynolds number ( $Re = 10^3, 5 \times 10^3, 10^4, 5 \times 10^4, 10^5, 5 \times 10^5, \text{ and } 10^6$ ). Pressure and velocity distributions over finite surface areas of NACA 2414 airfoil for different angles of attack and Reynolds number are presented. Aerodynamic performance coefficients are plotted against the angle of attack. Lift to Drag Ratio at various wind speeds of ( $u=0.001$  m/s, 1 m/s, 5 m/s, 10 m/s and 15 m/s) for the airfoil graph is plotted.

The results is clearly noticed that  $Cl/CD$  is linearly increases as the value of angle of attack is increased and after a certain angle of attack it is decreased and this angle is called stalling angle. The results showed that the effect of varying Reynolds number was important on aerodynamic performance and on pressure and velocity distributions over the surface of airfoil.

**Keywords:** *airfoil, lift and Drag Coefficients, Aerodynamics, Reynolds number, Angle of Attack*

## 1. Introduction

Fossil fuels is very important for human life and living environments but according to the US Department of energy, the combustion of fossil fuels results a net increase of 10 billion tons of atmospheric carbon dioxide every year which effects negatively the environmental balance.

Furthermore, these limited resources should meet the increasing demands of energy, estimates from the US Department of Energy predict that the years of production left in the ground for oil are 43 years, gas 167 years, and coal 417 years [1]. Therefore, it is critical that we start looking for some renewable sources of energy that can be used as alternatives to fossil fuels. Renewable energy resources can play a key role in producing clean, local, and unlimited energy to supply the growing demand for electricity. One of the renewable energy is wind energy, Wind turbines use wind energy to transform into electrical Energy, comparing other renewables wind power generation is the fastest growing industry in energy sector, by the end of 2012, the world total installed capacity of wind turbines reached 285 GW and it is expected to reach 500 GW in the year of 2017 [2]. Therefore, it is preferred widely as an alternative to fossil fuels and is widely distributed, and clean and produces no greenhouse gas emissions. Wind turbines convert kinetic energy from the wind into mechanical energy which can be used to generate electricity. One of the most important parameters of wind turbines is the blade because wind hits the blades, it generates lift forces which makes the blades spin. These blades are connected to a drive shaft that turns an electric generator to produce electricity which therefore can be sent through a cable down the turbine tower to a transmission line. In the literature, the imaginary of sectional blades profiles are called as airfoils. Airfoil profile is the important parameter for blade design because blade efficiency increases depending on airfoil profile, so there are a lot of studies over the airfoil profile as numerical and experimental in the literature. The aerodynamic profiles of wind turbine blades have crucial influence on aerodynamics efficiency.

Experimental investigations are very important due to accuracy. However, those take much time and economic and whenever we want to change a parameter about our study, it is very difficult because of time, economic and the risks of repeated experiments. Fortunately, researchers can study very fast and easily by using computational fluid dynamics (CFD) programs [3,4]. These programs can give as correct results as experimental method does. The wind turbine community has started to look at CFD methods to complement wind tunnel [5] and in field tests on the understanding of the complex flow physics around rotating wind turbine blades, there are number of researches have been conducted to increase size, efficiency, reliability of the wind turbines by reducing cost and complexity. In last decade, studies about aerodynamics simulation have been focused on, the compressible and incompressible Reynolds Averaged Navier-stokes (RANS) equations. These equations are coupled with turbulence models with various degree of complexity, zero equation models, such as the Baldwin-Lomax [6], while the one equation Spalar-Allaras turbulence model has also been quite popular [7]. Two equations models, such as the standard K- $\epsilon$  model are commonly used [8], modern models such as the K- $\omega$  SST [9] have been also employed in many aerodynamics matters.

NACA airfoil is designed generally for aircraft. Then, some designed airfoils have been also used in wind turbines. NACA-four digits airfoil or five digits types (National Advisory Committee for

Aeronautics) were investigated in the literature. Generally, a lot of researchers studied lift and drag performances of NACA airfoil. Habtamu and Yingxua., have computed aerodynamic performance analysis of a symmetric NACA0018 wind turbine airfoil by using numerical simulation method. The authors investigated lift, drag performances and surface pressure by changing attack angle using different turbulence model [10]. Bhat *et al.*, studied oscillating of NACA 0012 airfoils at around stall angle at low Reynolds number [11]. Lianbing *et al.* have investigated performance of wind turbine NACA0012 airfoil using Fluent programs. Spalart-Allmaras turbulence model to numerical solutions was used by Lianbing *et al.* of airfoil at  $3 \times 10^6$  Reynolds number for lift and drag performance and stall angle [12]. Villalpando *et al.* studied over NACA 63-415 airfoil profile using different turbulence model in Fluent and they have concluded that Spalart- Allmaras model was better than others models, they also investigated aerodynamics of airfoil at high and low angles of attack [13]. Ravi *et al.* studied over NACA4412 airfoil profile at  $3 \times 10^6$  Reynolds numbers, investigating transition from laminar flow to turbulence flow by using two different CFD models which were k- $\epsilon$  and Spalart Allmaras. CFD results were compared with experimental results, and gave similar results at high Reynolds number [14]. Lubitz investigated the effect of ambient turbulent levels on wind turbine energy production, the results have shown that ambient turbulent intensity had different impacts at different speed [15]. Srinivosan *et al.*, studied on evaluation of turbulence models for unsteady flows of an oscillating airfoil. NACA 0015 airfoils were used by five different turbulence model. It has seen that Spalart-Allmaras turbulence model had good agreement with experimental results for lift, drag and moment coefficient [16].

In the present work, the lift and drag performances of NACA 2414 wind turbine airfoil were investigated as numerical. In order to achieve this overall goal, several specific objectives were determined. The first specific objective was to identify several NACA 2414 airfoil profiles with their geometric coordinates. The second objective was to perform CFD Comsol Multiphasics simulations around the airfoils. Pressure distribution over the body surface for each airfoil was performed for laminar and turbulent flow. The third objective was to determine the results of airfoils subjected to different attack angles ( $\alpha$ ) and Reynolds numbers (Re). The calculation of lift coefficients (CL), drag coefficients (CD) and CL/CD ratio at different operating conditions will be determined.

## 2. Theoretical Background

---

The airfoil characteristics of the wind turbine defines the aerodynamic performance, amount of mechanical power of the rotor, and rigidity of the airfoil blade. It is important to understand the aerodynamic concepts of the airfoils to define the power production of the given wind turbine.

### 2.1. Structural Terminology

Typical air foil can be divided into four sections, the leading edge, trailing edge, upper surface or suction side, and lower surface or pressure side. the line connecting leading edge with trailing edge is called the chord line. the curve that passes through midway point of the upper surface and the lower surfaces of the airfoil is called mean camber line, the typical of airfoil structure is shown in Fig. 1

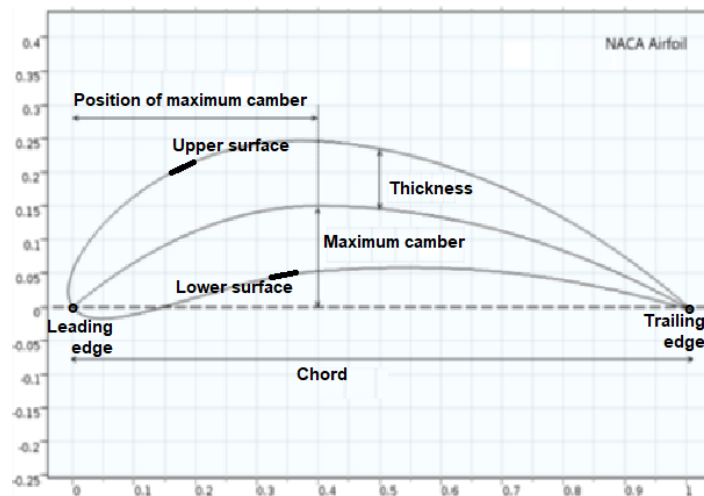


**Figure 1** Structure of the typical airfoil

## 2.2. Turbulent vs. Laminar Flow

When airflow with no disturbance and smooth streamline is called laminar flow. The particles of the air flows parallel layer and becomes increasingly laminar causing an increase in aerodynamic drag, and as a result reduces the aerodynamic efficiency of the airfoil. In turbulent flow, to simulate flow in laminar flow region by changing the fluid inlet velocity of the wind tunnel and estimating the Reynolds number. the fluctuations cause the particles of the air to get mixed and move through the layers; as a result they get high and low kinetic energy, giving a much more uniform velocity profile. Also, turbulent flow has higher friction and lower tendency to separate [17].

## 2.3. Reynolds Number

One of the important parameter for every airfoil is its operating Reynolds number, Reynolds number of the airfoil profile is defined as  $Re = \frac{UC}{\nu}$  where U is the relative velocity of wind. C is the chord length, and  $\nu$  is the kinematic viscosity. Hence, airfoils at different Reynolds number exhibit distinctive performance, directly affecting the aerodynamic design of wind turbine. The performance characteristics of an airfoil are expressed as a function of Reynolds number, and it significantly affects the values of airfoil drag and lift characteristics. The general level of the drag

coefficient increases with decreasing Reynolds number. The large Reynolds number tells that inertial forces are predominating than viscous forces.

## 2.4. Lift and Drag Forces

The airflow through an airfoil is distributed asymmetrically and creates forces on the airfoil surface. The force that works normal to the body is referred as lift force. When fluid incorporates a circulatory flow about the body then lift will create as velocity above the object is increased and static pressure is reduced. The lift force is obtained when there is a pressure difference of the air between upper surface region and the lower surface region of an airfoil. Drag force on a body is also a force as lift force but works in the direction parallel to the flow, and it is also created from unequal pressure on the airfoil surfaces facing forward and away from the oncoming flow. The lift force is a beneficial force, which needs to be increased, and the drag force needs to be as much as smaller in order to get high lift to drag ratio. The lift coefficient ( $C_L$ ), drag coefficient ( $C_D$ ) and lift to drag coefficient are important tools to measure the airfoil power performance.

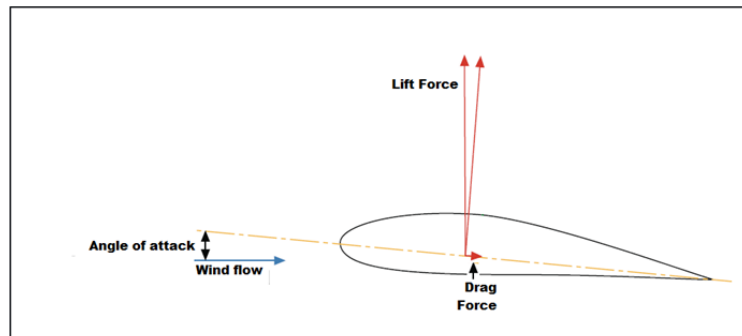


**Figure 2** Lift and drag forces, angle of attack

## 2.5. Angle of Attack, Separation, and Stall

Angle of attack  $\alpha$  is defined the angle between the w-direction at the leading edge and chord line of an aerofoil. The angle of attack can be positive or negative depending on the position and shape of an airfoil. When the flow is no longer manages to stay attached to the surface the separation will occur, where there will be a layer of reversed flow close to the surface, and oncoming flow will be pushed away. The magnitude of the lift and drag forces differ with the angle of attack. Lift force is high at small angles of attack but drag force is low for a certain angle of attack. After that lift force decreases where drag forces increases.. This certain angle called a stalling angle and from this angle the drag starts to increase dramatically reducing the lift.

### 3. CFD Modeling and Simulation

A segregated, implicit solver, Comsol Multiphasics, is utilized to simulate the problem. The airfoil profile is stimulated in the Design Modeler and boundary conditions, meshes are created. With the help with the commercial CFD software Comsol, two dimensional airfoil's aerodynamic performance was simulated numerically. The control equations were Navier-Stokes equations, with the Spalart–Allmaras turbulence model.

When you enter the fluid flow's Reynolds number into the simulation app, the appropriate fluid flow interfaces and meshes are automatically chosen based on this number. Low Reynolds number simulations are performed with the Laminar Flow interface, while high Reynolds number simulations use the Spalart-Allmaras turbulence model, which has been specifically developed for airfoil design simulations.

In this work, we consider the flow around NACA airfoil shape at 7 different Reynolds number ( $Re = 10^3, 5 \times 10^3, 10^4, 5 \times 10^4, 10^5, 5 \times 10^5, \text{ and } 10^6$ ) for a range of  $-5^\circ$  to  $15^\circ$  angles of attack.

#### 3.1 Geometry Generation

Bezier curve method [18] which uses thirteen control airfoil geometry parameters, these parameters can control local changes in upper and lower surfaces of airfoil. Other parameterization methods, include the PARSEC method [19], which uses eleven specific airfoil geometry parameters and the Bezier-PARSEC method [20] which combines the Bezier and PARSEC methods. In this study, for seeking of simplicity, we use the NACA 4-digits airfoil shapes as a parameterization method [21] where the airfoil shape is defined by three parameter, maximum upper camber,  $m$  (as percentage of the cord), the second parameter, the position of the maximum upper camber from the airfoil leading edge,  $p$  (as percentage of the cord), and the last parameter describes the maximum thickness of the airfoil ( $t/c$ ), as percent of the chord length. The airfoils are denoted by NACA  $mpxx$ , where  $xx$  is the thickness to the chord ratio  $t/c$ . since these parameters are widely accepted in aerodynamics airfoil designs and satisfy the conditions and the objectives of this study. The runner airfoils are shaped with NACA-2414 of airfoil of four digits.

The dimensionless coordinates  $(x, y)$  at the airfoil mean camber line for NACA-4digits is defined in a piecewise manner as

$$y_c = \frac{m}{p^2}(2P^2x - x^2) \quad \text{for } 0 \leq x < p \text{ and}$$

$$y_c = \frac{m}{(1-p)^2}((1 - 2p) + 2Px - x^2) \quad \text{for } p \leq x \leq 1$$

$y_t$  is the half thickness distribution for a symmetric NACA-4digit of airfoil with maximum thickness to chord ratio for a given  $x$  value

$$y_t = \pm 5 tc(0.2969\sqrt{x} - 0.1260x - 0.3516x^2 + 0.2843x^3 - 0.1015x^4)$$

We assume the mean chord length  $C=1$ . The relative thickness of airfoil equals 14%, and the dimensionless maximum upper camber  $m$  ( as percentage of the chord,  $(\frac{m}{c})$ , Its value as

percentage of the chord equals 2%, and its position  $p$  equals 40% of the chord. The total coordinates  $(x, y)$  at the upper and lower surfaces at the NACA airfoil are defined by

$$y_{upper} = y_c + y_t \cos(\theta(x)) \quad y_{lower} = y_c - y_t \cos(\theta(x))$$

$$x_{upper} = x - y_t \sin(\theta(x)) \quad x_{lower} = x + y_t \sin(\theta(x))$$

Where

$$\theta(x) = \begin{cases} \tan^{-1}\left(\frac{2m}{P}(P-x)\right) & x < P \\ \tan^{-1}\left(\frac{2m}{(1-P)}(P-x)^2\right) & x \geq P \end{cases}$$

### 3.2 Blade Airfoil and Parameters

The physical parameters of primary air are used in the simulation as follows: Air velocity is 5 m/s, atmospheric pressure is 101325 Pa, air density is 1.225 kg/m, air temperature is 293 K, kinematic viscosity is  $1.82 \times 10^{-5}$  m<sup>2</sup>/s. compressible flow ( $M_a < 0.3$ ), Turbulence model RANS, Turbulence model type is Spalar-Allaras.

**Table 1** Parameters of NACA 2414

Parameters	Values
Chord length, C	1
Maximum camber, m	0.02
Position of the maximum camber, P	0.4
Maximum thickness, t	0.14
Wind speed, u	5
Angle of attack, $\alpha$	0°
Reynolds Number, Re	$1 \times 10^5$
Computational domain, $n_r$	10
Density Dynamics viscosity,	$\frac{1}{Re}$

### 3.3 Size of Computational Domain

The computational domain is located 10 chord length away from leading edge and 20 chord length away from trailing edge. The far field is divided into two regions, a semi-circle and rectangular, so that the inlet can have a prescribed velocity boundary condition while pressure is prescribed at the outlet. Choosing small distance to reduce computational time and the distance suggested is enough. Simulations are performed with various different domain sizes. The lift and drag coefficients ( $C_L$  and  $C_D$  respectively) as a function of domain size are presented in Fig. 3. It can be observed that the lift to drag ratio ( $\frac{C_L}{C_D}$ ) and therefore the airfoil performance requires a larger domain than initially thought to be independent of the far field. With that in mind, the grid to be used in the subsequent simulations has a distance between the airfoil and the external boundaries of about 100 chord by Mavriplis et al [22]

If a CFD boundary with a specified far field pressure boundary condition is placed too close to the airfoil, its enforcement of the pressure will be felt through the flow field, causing the pressure distribution near the body to be inaccurate. The domain can also be too large with an unnecessary number of cells that increase simulation time. Setting these boundary conditions an appropriate distance away from the model increases the chance that any error in the initial estimation will be dissipated before reaching the body.

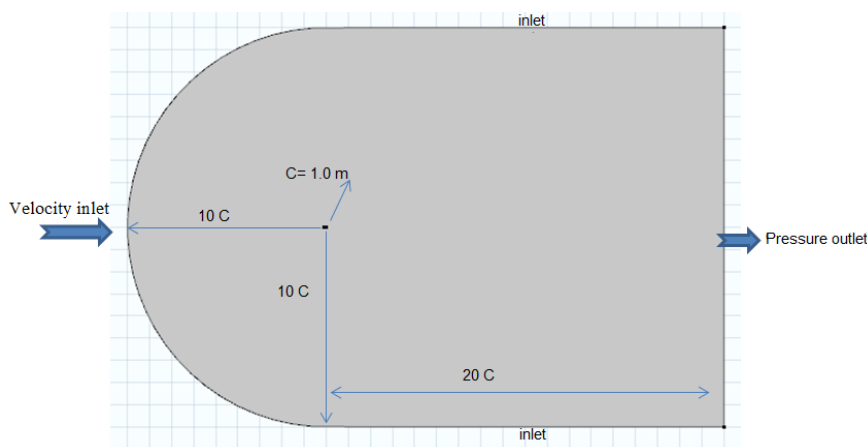


**Figure 3** Computational domain of CFD model

### 3.4 Airfoil Grid Meshing

The simulation of the blade airfoil begins with the airfoil calculating field firstly. The appropriate selection of the calculation of the flow area has an important influence on the simulation results. In principle, the boundary is as far as possible [23], but it also increases the amount of computation

and the result may not be the best. According to the experiences of predecessors [24] the selected airfoil grid shape is free C-shape which can make the mesh generation convenient. The free (unstructured) meshing method is used to mesh the airfoil grid, the unstructured meshing method has been also used to mesh the airfoil grid by Lindenburg [25]. The mesh is calibrated for fluid dynamics models. In this study, two size of meshes are used to mesh the entire domain and boundaries of airfoil for turbulent and laminar flow, Low Reynolds number simulations are performed on a coarse mesh with the Laminar Flow interface in the CFD Module while high Reynolds number simulations are performed on a fine mesh with the Turbulent Flow interface in the CFD Module. The resolution and density of the mesh is more condensed in regions where superior computational accuracy is needed, such as the near wall region of the airfoil. In high quality unstructured grid is shown in Fig. 4a and Fig. 4b, the integral mesh grid of the flow field of wind turbine blade airfoil in both cases of turbulent and laminar.

**Table 2.** The integral mesh grid

<b>Meshes</b>	<b>Size 1</b>	<b>Size2</b>
Mesh1 Turbulence	Domain Elements Fine 10257 elements $0.02 < size < 0.7$	Boundary Elements Finer 209 elements $0.008 < size < 0.56$
Mesh2 Laminar	Domain Elements Coarse 3185 elements $0.06 < size < 1.34$	Boundary Elements Fine 111 elements $0.02 < size < 0.7$

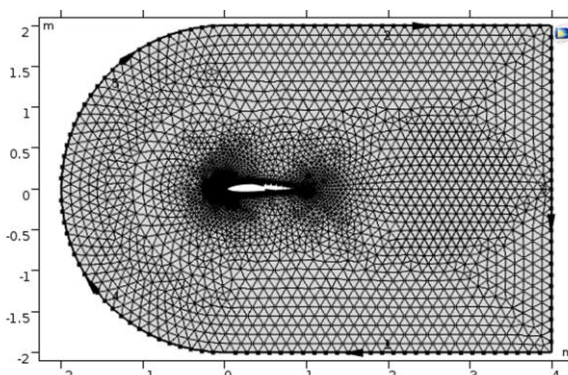


**Figure 4a** Mesh 1 for turbulent air flow

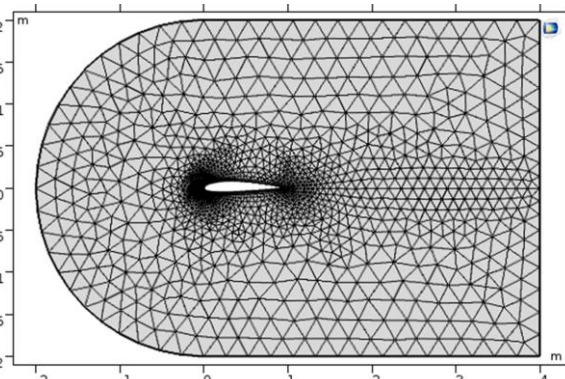


**Figure 4b** Mesh 2 for laminar air flow

## 4. Results and Discussion

### 4.1 Pressure Distribution

Fig. 5a shows the outcomes of static pressure of laminar model ( $Re=10^3$ ) and Fig. 5b shows the outcomes of static pressure of turbulent model ( $Re=10^6$ ) at angle of attack  $0^\circ$ . It is shown from the figures 5a and 5b that, magnitude of pressure on the airfoil is less in upper surface than that of the incoming flow stream. As a result an effective upward push called lift is obtained, perpendicular to the incoming flow stream. Laminar flow becomes go through transition turbulence flow.

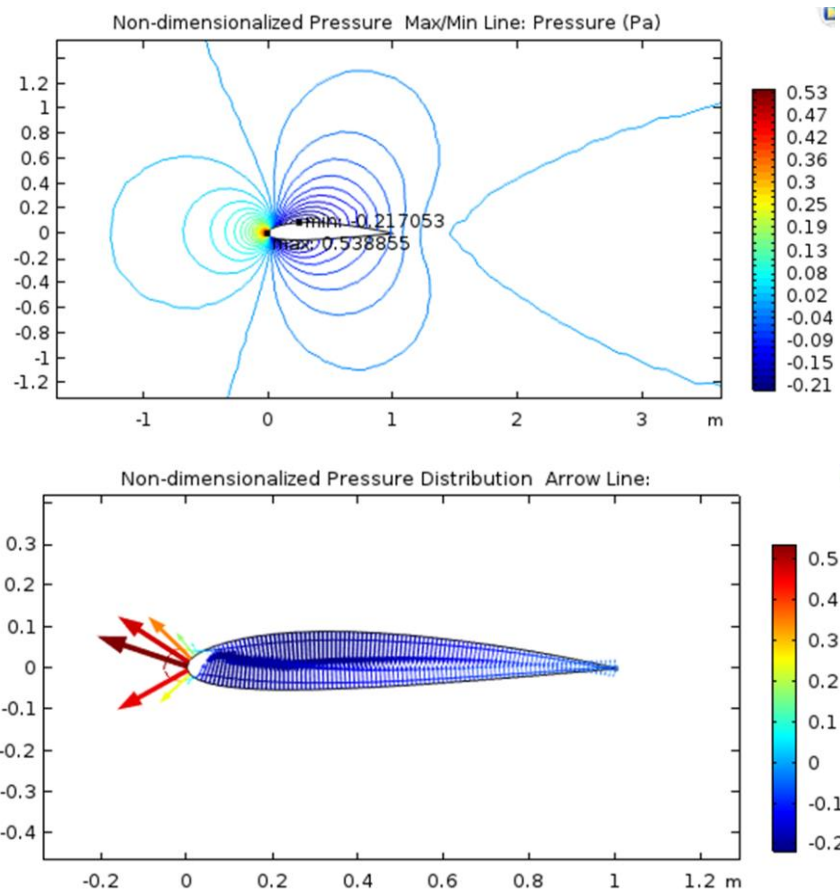


**Figure 5a** Pressure distribution (laminar  $Re=10^3$ )

The pressure coefficient of the airfoil upper surface was negative and the lower surface was positive in laminar and turbulent model. Thus the lift forces of the airfoil is in the upward of pressure between the lower and upper surfaces. It can be observed that pressure contour in laminar flow similar and symmetric around airfoil

We can see also that the pressure difference is much larger on the leading edge, reddish color, while the trailing edge it was much lower. Thus indicating that the lift force airfoil is mainly generated from the front edge. From the contour of pressure coefficient; it is shown that there is a region of high pressure at the leading edge (stagnation point) and region of low pressure on the upper surface of airfoil. Yellowish color in the upper

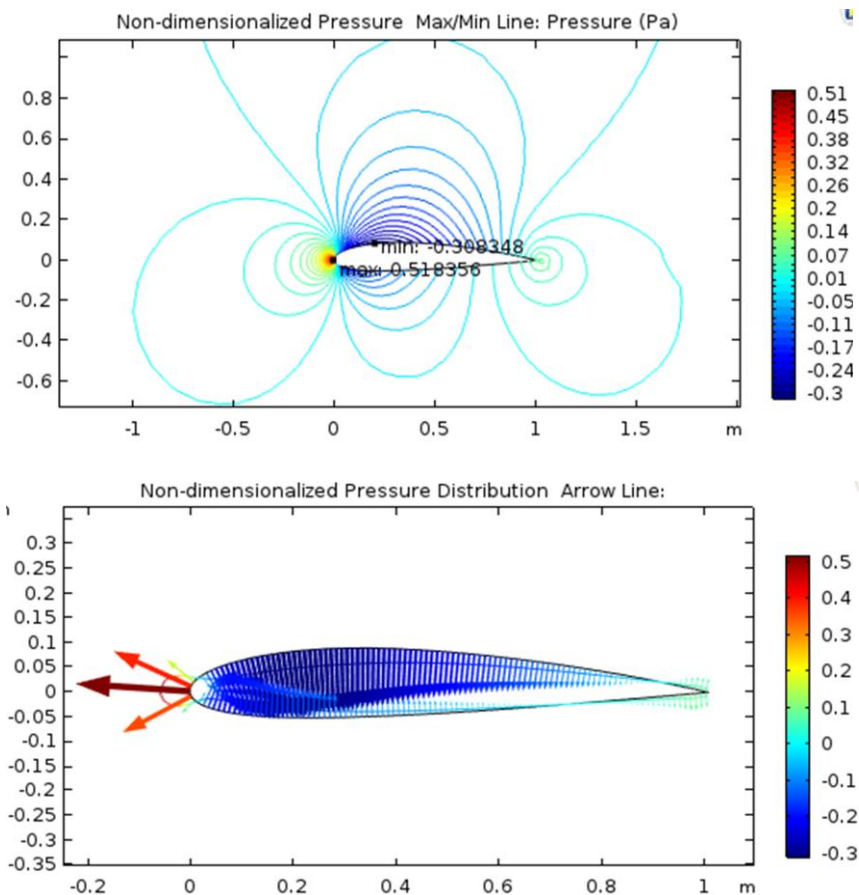


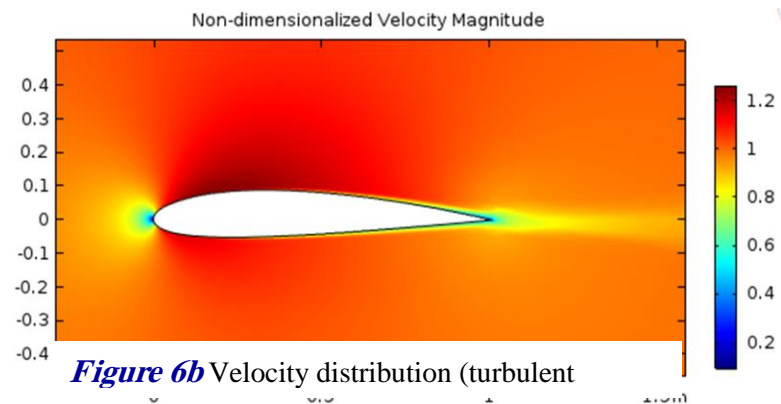
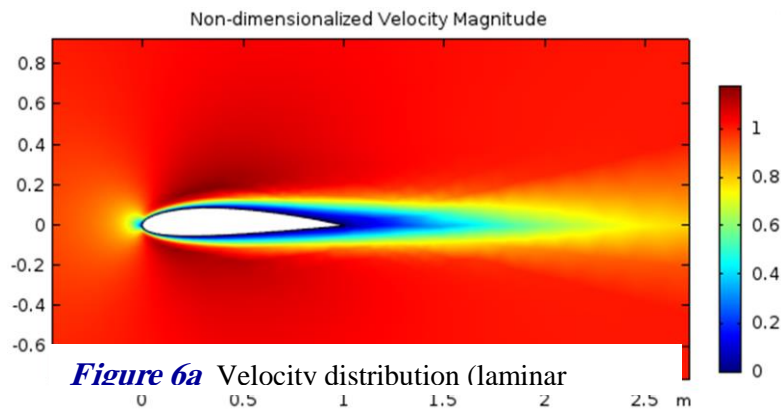
**Figure 5b** Pressure distribution (turbulent

portion of the airfoil, the fluid velocity increases and low pressure is created and the lift force acts upwards to rotate the rotor. In turbulent model, a circulation region of the trailing edge portion of the airfoil where eddy currents are formed and flows are pushed away from body. This results flow separation and related change in pressure distribution around airfoil manifest itself as pressure drag. This situation negatively affects the lift coefficient. At stagnation point pressure is maximum and velocity is zero which is characterized by distinct blue point on the velocity contour plots. It is also apparent in laminar that with zero angle of attack separation layer moves toward trailing edge

on the lower and upper surfaces of the airfoil which creates significant amount of positive drag, while in turbulent, the pressure deviation on the upper and lower surface of the airfoil principally creates significant amount of positive lift.

## 4.2 Contours of Velocity Magnitude

The pressure difference that has previously appeared is accompanied by a velocity difference, via Bernoulli's principle, so the resulting flow field about the airfoil has a higher average velocity on the upper surface than on the lower surface. velocity distribution show that static pressure increases at the lower surface of the airfoil but reversely velocity magnitude increases at the upper surface.



Velocity components at angles of attack  $0^\circ$  are also shown in Fig. 6. Higher velocity is experienced in the upper surface compare to lower surface and increase as expected from the nature of pressure

distribution. The Fig. 6(a) shows that trailing edge of airfoil experiences lower velocity than leading edge. It is clearly noticed from the Fig. 6(a) that velocity is symmetrical and creates separation layers at the boundaries of airfoil towards the trailing edge, bluish color, which creates a significant amounts of drag forces. It is clearly noticed from the Fig. 6(b) , it can be seen on the leading edge a stagnation point where the velocity of the flow is nearly zero. The fluid accelerates on the upper surface as can be seen from the change in colors of the contour into dark red color which generates more lift. It can be seen also disappearing of blue layer and all layers of air were mixed in turbulent model.

### 4.3 The Effect of Wind Speed

Figure 7 shows Lift to Drag Ratio,  $\frac{C_L}{C_D}$  at various wind speeds of 0.001 m/s, 1 m/s, 5 m/s, 10 m/s and 15 m/s for the airfoil. Notice in Fig. 7, that the wind turbines have different cut-in velocities, as well as different design powers performance. These parameters are very important in choosing the wind turbine for a specific installation site. Notice in Fig. 7, that each wind turbine has different design torques (for different wind speeds) varying according to geometrical similarity coefficients.

**Table 3.** varying in lift to drag ratio to wind speed

Wind Speed, $\frac{m}{sec}$	Lift to Drag Ratio, $\frac{C_L}{C_D}$
0.001	0.0417
1	9.088
5	11.77
10	13.87
15	16.04

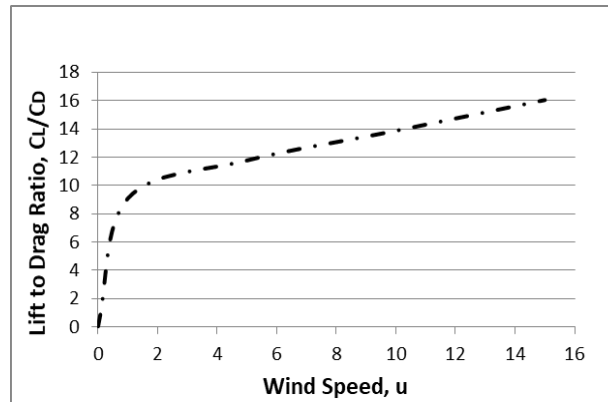


**Figure 7.** Variation of lift to drag ratio to wind speed

#### 4.4 Lift and Drag Coefficients Versus Angle of Attack

Lift and drag coefficients depend on angle of attack. The experimental results obtained from our airfoil model are plotted on graph. The Fig. 8a shows that lift coefficient at low angle of attack increases linearly with increasing angle of attack and after a certain angle of attack it is decreased, such as a higher lift coefficient, a lower drag coefficient was noticed as shown in Fig. 8b which induces on maximum lift to drag ratio at a given angle of attack which located between the maximum lift and minimum drag coefficients and this angle is called stall angle.

CL is maximum (29.69) at  $10^\circ$ . The stall angle is caused transition from laminar to turbulence flow. Drag coefficient also depends on angle of attack. It is clear from Fig. 8b that the value drag coefficient is increased as angle of attack is increased. Drag coefficient is minimum (0.2627) at  $0^\circ$ .

From Fig. 8c it is clearly noticed that  $CL/CD$  is gradually increases as the value of angle of attack is increased.  $CL/CD$  is maximum (43.29) at  $5^\circ$ . After these values  $CL/CD$  ratio start decreases with the increases of angle of attack.

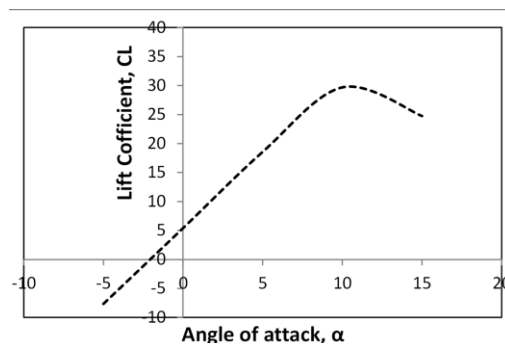


**Figure. 8a** Variation of the coefficient of lift to the angle of attack

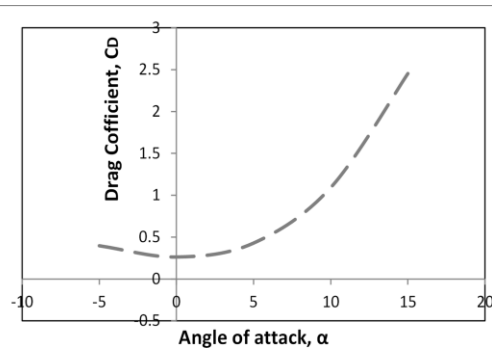


**Figure. 8b** Variation of the coefficient of drag to the angle of attack

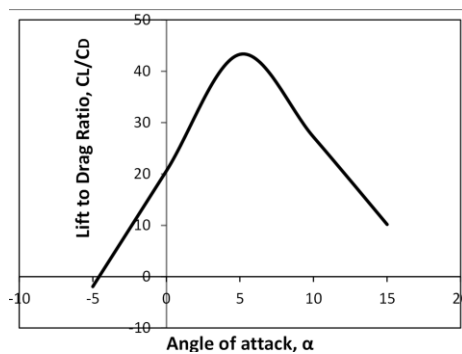


**Figure. 8c** Variation of  $C_L/C_D$  w.r.to Angle of attack

### 4.5 Lift and Drag Coefficients Versus Reynolds Number

Six Reynolds numbers varying from  $10^5$  to  $10^6$ , which cover most wind turbines in turbulent mode, all of the turbine rotors exhibit better performance, such as a higher lift coefficients CL which increases linearly beyond Reynolds of  $5 \times 10^5$  as shown in Fig. 9a. The drag behavior is highly depends on Reynolds number, especially in low values, it is shown in Fig 7b that drag at lower Re numbers gain higher values, a drag coefficient decreases rapidly then reducing at slower rate beyond  $Re = 5 \times 10^5$ , this inducing a larger lift to drag at higher Reynolds number as shown in Fig. 9c, it was also previously observed that increasing Reynolds number the boundary layers becomes thinner and the fluid around the airfoil turbulent and more powerful.

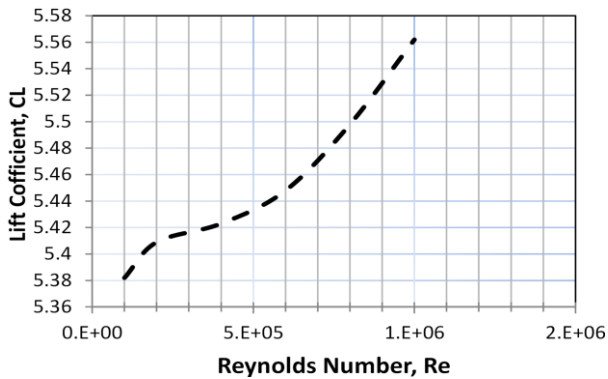


**Figure. 9a** Variation of the coefficient of lift to Reynolds number

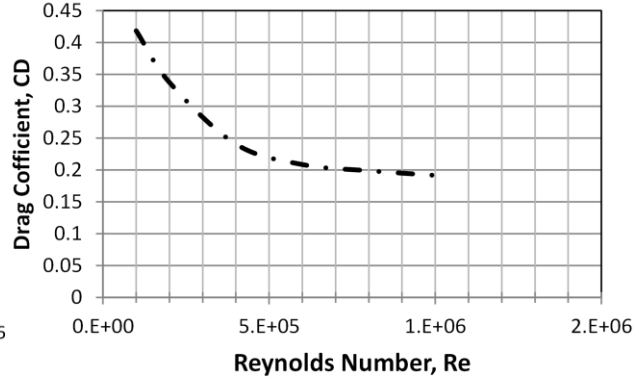


**Figure. 9b** Variation of the coefficient of drag to Reynolds number

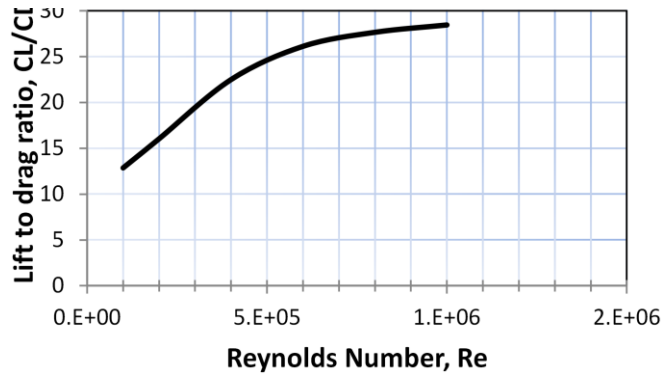


**Figure. 9c** Variation of the coefficient of lift to drag ratio to Reynolds number

## 5. Conclusions

---

With the help of CFD software Comsol Multiphasics, successful analysis of the aerodynamic performance of NACA 2414 airfoil has been carried at various angles of attack ( $\alpha = -5, 0, 5, 10, 15, 15$  degrees) with constant Reynolds number ( $10^5$ ) and it has been also carried at various Reynolds number  $Re = 10^3, 5 \times 10^3, 10^4, 5 \times 10^4, 10^5, 5 \times 10^5, \text{ and } 10^6$ ) with constant angles of attack (0 degree) using the Spalar-Allaras turbulence model. The pressure of the airfoil's upper surface was negative and the lower surface was positive, thus the lift force of the airfoil is in the upward direction. The coefficient of pressure difference is much larger on the leading edge, while on the trailing edge it was much lower. The lift forces were increased as the angle of attack increased until a certain value of angle then it is decreased and this angle is called a stalling angle. It is concluded that the best aerodynamic performance was happened at 5 degree of angle of attack. The results concluded also that the lift to drag ratio was increased as the wind speeds and Reynolds number increased.

## References

---

- [1] worldwide look at Reserves and Production (2008) Oil & Gas J. 106 (48):23-24
- [2] "Navigant Research." Navigant Research World Market Update 2012 Comments. Web. 08 Nov. 2013.
- [3] A. M. Muftah "3D Fluid in an Elbow Meter-CFD Model" SUSJ Journal, Sirte University, Vol. 4, Issue 1, June 2014
- [4] A. Muftah "CFD Modeling of Elbow and Orifice Meters" SUSJ Journal, Sirte University, Vol. 7, Issue 1, June 2017, pp 15-32
- [5] K. S. Patel, S. B. Patel, U. B. Patel, and A. P. Ahuja, "CFD Analysis of an Aerofoil", International Journal of Engineering Research, vol. 3, issue. 3, pp. 154-158, March 2014.
- [6] B.S. Baldwin, H. Lomax: "Thin-layer approximation and algebraic model for separated turbulent flows". AIAA Paper No. 78-257, 1978.
- [7] P. R. Spalart, Allmaras, S., "A One-equation Turbulence Model for Aerodynamic Fows," AIAA-92-0439, 1992.\
- [8] D. C. Wilcox, *Turbulence Modeling for CFD*. Canada: Industries, Inc., pp. 103-218, 1998.
- [9] F.R. Menter: "Two-equation eddy-viscosity transport turbulence model for engineering applications". AIAA Journal, Vol. 32, 1994, pp. 1598-1605
- [10] B. Habtamu, and Y. Yingxua, "Numerical Simulation of Unsteady Flow to Show Self Starting of Veritcal Axis Wind Turbine Using Fluent", Journal of Applied Sciences, Vol. 11, 2011, pp. 962–970.
- [11] Shantanu S. Bhat, Raghuraman N. Govardhan, "Stall flutter of NACA0012 airfoil at low Reynolds numbers ", Journal of Fluids and Structures 41 (2013)166–174

- [12] L. B. Li, Y. W. Ma, and L. Liu, "Numerical simulation on aerodynamics performance of wind turbine airfoil," in *Proc. World Automation Congress (WAC)*, 2012, pp. 1-4.
- [13] F. Villalpanda, M. Reggio, and A. Ilinca, "Assessment of turbulence model for flow simulation around a wind turbine airfoil," *Modeling and Simulation in Engineering*, February 2011.
- [14] H. C. Ravi, N. Madhukeshwara, and S. Kumarappa, "Numerical investigation of flow transition for NACA-4412 airfoil using computational fluid dynamics," *International Journal of Innovative Research in Science Engineering and Technology*, vol. 2, issue 7, pp. 2778-2785, July 2013.
- [15] Lubitz WD. Impact of ambient turbulence on performance of a small wind turbine. *Renewable Energy* 2014; 61:69–73.
- [16] G. R. Srinivasan, J. A. Ekaterinaris, and W. J. McCroskey. Evaluation of Turbulence Models for Unsteady Flows of an Oscillating Airfoil. *Computers & Fluids*, 24(7):833-61, Sept. 1995
- [17] E. Saeta and P.Krogstad. Design of Airfoil for downwind wind turbine Rotor. Master of Sciences in Engineering. Norwegian University of Science and Technology. June, 2009
- [18] peigin, S.E., Epstein, B.: Robust Optimization of 2D Airfoils Driven by Full Navier-Stokes Computations. *Computers & Fluids*. 33, 1175-1200 (2004)
- [19] Sobieczky, H.: Parametric Airfoils and Wings. In. Fuji. K., Dulikravich, G.5.(EDS) Notes on Numerical Fluid Mechanics. Vol 68. Wiesbaden, Viewing (1998)
- [20] Derksen, R. W., Rogalsky, T.: Bezier-PARSEC. An optimized Airfoil parameterization for Design. *Advances in Engineering Software*, 41, 923-930 (2010)
- [21] Abbott, I.H., Von Doenhoff A.E. *Theory of Wing Sections*. Dover publications. Newyork (1959)
- [22] D. Mavriplis, J.C. Vassberg, E.N. Tinoco, M. Mani, O.P. Brodersen, B. Eisfeld, R.A. Wahls, J.H. Morrison, T. Zickuhr, D. Levy, M. Murayama, Grid Quality and Resolution Issues from the Drag Prediction Workshop Series, *J. Aircr.* 46 (3) (2009) 935–950
- [23] Hand M. M., Simms D. A. Unsteady aerodynamics experiment phase VI: wind tunnel test configurations and available data campaigns. National Renewable Energy Laboratory, Technical reportr, NREL/ TP 2500-29955, 2001.
- [24] Schepers J. G., Feigl L., Rooij R. V., Bruining A. Analysis of detailed aerodynamic field measurements using results from an aeroelastic code. *Wind Energy*, Vol. 7, Issue 4, 2004, p. 357-372
- [25] Lindenburt C. Investigation into rotor blade aerodynamics. Report Number ECN-C-03-025, 2003.